Theoretical considerations for mapping activation in human cardiac fibrillation

Wouter-Jan Rappel[1,2] and Sanjiv M. Narayan[3,4]
[1]*Department of Physics, University of California, San Diego, California 92093, USA*
[2]*Center for Theoretical Biological Physics, University of California, San Diego, California 92093, USA*
[3]*Department of Medicine (Cardiology), University of California and Veterans Administration Medical Centers, San Diego, California 92161, USA*
[4]*Institute for Computational Medicine, University of California San Diego, California 92161, USA*

(Received 4 March 2013; accepted 1 May 2013; published online 23 May 2013)

Defining mechanisms for cardiac fibrillation is challenging because, in contrast to other arrhythmias, fibrillation exhibits complex non-repeatability in spatiotemporal activation but paradoxically exhibits conserved spatial gradients in rate, dominant frequency, and electrical propagation. Unlike animal models, in which fibrillation can be mapped at high spatial and temporal resolution using optical dyes or arrays of contact electrodes, mapping of cardiac fibrillation in patients is constrained practically to lower resolutions or smaller fields-of-view. In many animal models, atrial fibrillation is maintained by localized electrical rotors and focal sources. However, until recently, few studies had revealed localized sources in human fibrillation, so that the impact of mapping constraints on the ability to identify rotors or focal sources in humans was not described. Here, we determine the minimum spatial and temporal resolutions theoretically required to detect rigidly rotating spiral waves and focal sources, then extend these requirements for spiral waves in computer simulations. Finally, we apply our results to clinical data acquired during human atrial fibrillation using a novel technique termed focal impulse and rotor mapping (FIRM). Our results provide theoretical justification and clinical demonstration that FIRM meets the spatio-temporal resolution requirements to reliably identify rotors and focal sources for human atrial fibrillation.
[http://dx.doi.org/10.1063/1.4807098]

Atrial fibrillation (AF) is the most common heart rhythm disorder (cardiac arrhythmia) in the United States that may cause substantial morbidity and mortality. However, the precise mechanisms causing AF are still not well understood, partly due to difficulties in reliably mapping electrical activity during the spatio-temporal variations of AF in patients. In this article, we determine the minimal spatial and temporal resolution required to accurately map in humans the electrical rotors and focal sources shown to sustain AF in various model systems. We first test these requirements in computer simulations. We then validate that a recently developed mapping technique which employs bi-atrial multielectrode contact arrays is able to capture localized rotors and focal sources for human AF.

I. INTRODUCTION

During normal sinus rhythm, an electrical wave initiated from the sinus node propagates through atrial tissue, activates the atrioventricular node then ventricular tissue, and resulting in coherent electrical activity and mechanical contraction (systole) in the heart. In a large number of people, however, this organized rhythm is disrupted and replaced by an arrhythmia during which wave propagation is fast and/or irregular and may compromise the primary mechanical function of the heart. AF is the most common of these arrhythmias and currently affects 5 million people in the USA alone. AF is a serious health concern and leads to increased morbidity and even mortality.[1]

The precise mechanisms that initiate and maintain human AF are not well understood. Part of the reason for this incomplete understanding is the difficulty in obtaining accurate human maps of spatio-temporally varying electrical activity in AF, and hence explaining consistent spatial gradients in rate and dominant frequency[2] and electrical propagation.[3] High resolution mapping techniques, especially ones using optical dyes, have proven to be instrumental in determining the spatio-temporal wave organization in animal models and in explanted human hearts.[4,5] Such models have shown that spatiotemporally variable AF may actually result from periodic sources in the form of spiral waves (electrical rotors)[6,7] or focal sources, in which activation spreads from an origin,[8] that are localized yet lie in unpredictable locations and thus are ideally identified using a wide field of view. In patients, optical techniques are not feasible due to the toxicity of dyes and, in the absence of other high resolution and wide field of view mapping studies, it is has not been defined to what extent animal data can be legitimately translated to humans.[6,7] Thus, to understand human AF and develop novel therapeutic interventions, it is critical to obtain reliable maps of electrical activity during AF in patients using clinically feasible methodologies.

Optical techniques provide a spatial resolution Δx of approximately 0.1 mm and a temporal resolution Δt of 1 ms and have been used to resolve electrical rotors and focal sources that sustain AF in animal models.[9,10] Arrays of

contact electrodes have been applied to study human AF, with electrode separation varying from 1–5 mm.[11,12] Mapping wide fields of view in animal studies is achieved in isolated heart preparations, while human mapping has been achieved either using contact electrode plaques on regions of the heart accessible during open heart surgery or using relatively few electrodes at percutaneous electrophysiology study.[13,14] Despite these studies, however, the mechanisms of human AF remain highly controversial,[7,15] and AF therapy has not advanced significantly in several years.[11,16]

Ideally, human AF would be mapped *in situ* during clinical electrophysiologic study to avoid open heart surgery while enabling direct therapy (ablation) based upon patient-specific mapping results.[1] It is often suggested that human AF mapping requires high spatiotemporal resolution with narrow field of view,[7,17] as in prior open-heart studies, rather than wide-field of view with moderate spatial resolution that is readily achievable by percutaneous methods. If true, this would essentially preclude mapping of human AF at clinical electrophysiologic study with its attendant benefits and opportunities for patient-tailored mechanistic therapy.

In this study, we therefore address the theoretical requirements to map in humans the spiral wave reentry (electrical rotors) or focal sources that sustain AF in several animal models.[9,10] We consider only the case of recording electrodes and not the effects of pacing in non-fibrillatory rhythms.[18,19] After providing theoretical estimates for the required spatial and temporal resolution, we determine the resolution requirements in computational electrophysiological models. We then examine spatio-temporal patterns in human AF obtained from our recently developed technique (focal impulse and rotor mapping, FIRM) that uses 128 contact electrodes in both atria at clinical electrophysiologic study.[12,20,21] Our results from each line of investigation indicate that the resolution provided by this technique is sufficient to capture rotors and focal sources for human AF.

II. THEORETICAL ESTIMATES

A. Geometric considerations

1. Mapping spiral waves

An analytical solution for the shape of a spiral wave in cardiac tissue is not available. To determine the minimum required resolution of a mapping system, however, we can approximate the wave front as an Archimedean spiral, which is written in polar coordinates (r,θ) as

$$r(\theta) = \frac{\lambda_{spiral}\theta}{2\pi}, \tag{1}$$

where we have taken for simplicity the spiral tip at r = 0 and where the wavelength λ_{spiral} determines the spatial separation between two successive arms of the spiral. This definition of wavelength differs from the clinical usage where it is defined as the product of the conduction velocity and the effective refractory period.[22] To illustrate the validity of this approach, we generated a spiral wave using a computer model that simulates wave propagation in an isotropic 2D sheet using the monodomain equation

$$\frac{dV}{dt} = \nabla \cdot D\nabla V - \frac{I_{ion}}{C_m}. \tag{2}$$

Here, V is the membrane voltage, $C_m = 1\ \mu\text{F/cm}^2$ represents the membrane capacitance, D is the diffusion tensor with diagonal entries of $D = 0.001\ \text{cm}^2/\text{ms}$, and I_{ion} represents the membrane currents. Given the need only to create *in silico* activation patterns, these membrane currents were implemented by the Fenton-Karma (FK) model.[23,24] Equation (2) was simulated using a standard finite difference scheme with a spatial discretization of 0.025 cm or 0.05 cm and a time step of 0.01 ms. Fig. 1(a) shows a resulting counterclockwise rotating spiral, visualized using a gray scale with white corresponding to depolarized (active) and black corresponding to repolarized (inactive) regions of tissue. In Fig. 1(a), we have also plotted as a red line the Archimedean spiral that fits the activation front of the numerically obtained spiral wave. As can be seen from this figure, the simple geometric shape approximates the spiral wave very well. Thus, a rigidly counterclockwise rotating spiral with a tip location of (0,0), uniform angular frequency ω, and period $\tau = 2\pi/\omega$ can be accurately described in Cartesian coordinates by

$$\begin{aligned} x &= \frac{\lambda_{spiral}\theta}{2\pi}\cos(\theta + \omega t), \\ y &= \frac{\lambda_{spiral}\theta}{2\pi}\sin(\theta + \omega t), \end{aligned} \tag{3}$$

where we have omitted an arbitrary phase constant.

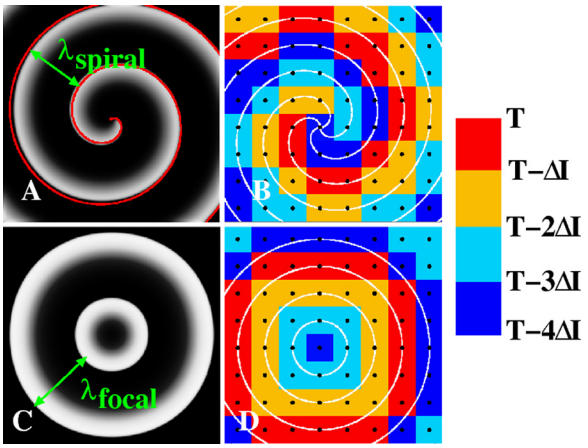

FIG. 1. (A) Computer simulation of a spiral wave using the Fenton-Karma model (parameter set #1 from Ref. 24). Activation is plotted in all figures using a gray scale with white corresponding to depolarized tissue and black corresponding to repolarized tissue. The wavelength λ_{spiral} of the rotor indicates the spatial scale between successive arms of the spiral. The red curve is an Archimedean spiral with its wavelength adjusted such that it fits the activation front of the simulated spiral. (B) Isochrones of a rigidly rotating Archimedean spiral with a period τ and separated by $\tau/4$ (white lines) and a square grid of electrodes with spatial discretization Δx (black dots). The wavelength of the spiral is $\lambda_{\text{spiral}} = 4\Delta x$ and the corresponding spatially continuous isochronal regions at time t = T are shown using the indicated color-scheme and time interval $\Delta I = \tau/4$. For larger spatial resolution, the isochronal regions are no longer spatially continuous. (C) Computer simulation of a focal source with a wavelength λ_{focal} and period τ using the same gray scale and parameter set as in (A). (D) Isochronal map of the focal beat of (C), along with isochrones separated by $\tau/4$ (white lines), computed from a square grid with resolution Δx.

The spatio-temporal organization in experimental and clinical data is often displayed using isochronal maps. These maps display regions of space that are activated within the same time interval ΔI. The boundaries between these isochronal regions are commonly referred to as isochrones. If we choose N time intervals of duration $\Delta I = \tau/N$, the boundaries between region n–1 and region n for the Archimedean spiral, again omitting a phase constant, is given in Cartesian coordinates by

$$x = \frac{\lambda_{spiral}\theta}{2\pi}\cos\left(\theta + \frac{2\pi n}{N}\right)$$
$$y = \frac{\lambda_{spiral}\theta}{2\pi}\sin\left(\theta + \frac{2\pi n}{N}\right) \quad (4)$$

and the distance between successive isochrones is found to be λ_{spiral}/N.

Suppose now that we have a square grid with grid spacing Δx. Then, the activation times (for a spiral wave with a tip at (0,0)) of electrode i at grid location x_i and y_i can be found as

$$t_i = \frac{\text{atan}\left(\frac{y_i}{x_i}\right) - \theta_0}{\omega} + \frac{2\pi k}{\omega}(k = 0, 1, ...), \quad (5)$$

where θ_0 is given by $\theta_0 = 2\pi\sqrt{x_i^2 + y_i^2}/\lambda_{spiral}$. From these activation times, it is straightforward to work backwards and to compute isochronal maps as is shown in the isochronal snapshot of Fig. 1(b). Here, we have chosen $N = 4$ and a spiral with a wavelength of $\lambda_{spiral} = 4\Delta x$. The analytical (Archimedean) boundaries between these regions are plotted in white and the electrodes, forming an 8×8 electrode grid, are shown as black circles. The $N = 4$ isochronal regions, computed using this grid, are shown using a color scale with all points that are activated in the isochronal interval $\Delta I = \tau/4$ immediately preceding the snapshot shown in red. If we denote the time of the snapshot by T, this corresponds to all points activated in the time interval (T- ΔI,T). Points activated in successively earlier isochronal intervals are colored as shown in the color bar.

Demanding that all isochronal regions are spatially continuous leads to a resolution requirement for the identification of a spiral wave using a discrete electrode grid. In other words, an isochronal region should be drawn such that an electrode belonging to this region is the nearest or next-nearest neighbor of other electrodes that are part of the same region. Clearly, such a region can no longer be drawn as the wavelength becomes smaller or, equivalently, if the distance between electrodes becomes larger. Note that this requirement will likely lead to a required spatial resolution that is too small as it might be possible to visually identify spiral waves for larger spatial discretization using isochronal regions that are only partially spatially continuous. This stringent condition can be translated into a required spatial resolution for the Archimedean spiral: spatially continuous isochronal regions are only possible for a spatial discretization that is equal or smaller that the distance between successive isochrones. Thus, the required spatial discretization, and the maximum spacing between electrodes, is

$$\Delta x_{max} = \lambda_{spiral}/N. \quad (6)$$

For smaller spatial discretization, the isochronal regions will be spatially continuous while for larger spatial discretization, they will no longer be spatially continuous. Of note, this requirement implies that the spatial requirements for large values of N, corresponding to a smaller time interval between successive isochrones as has become customary in the literature, are more demanding than for small values of N.

This analysis is only valid for reentry patterns that have a non-meandering core with a negligible size. A more complicated spiral tip trajectory introduces a new length scale in the problem, L_{tip}, which represents the spatial scale of the spiral tip path. Clearly, to accurately map the spiral tip path requires a spatial resolution smaller than L_{tip}, although the precise requirement depends on the complexity of the path. For complex paths, corresponding to rotors whose cores show spatial precession such as in AF,[25] the required resolution to map the spiral tip path may be much smaller than L_{tip}.

An additional length scale can be defined as the size of the coherent domain of the spiral wave, L_{rotor}. Within this domain, the rotor controls tissue activation in a 1:1 fashion; while beyond it, the rotor destabilizes and breaks down ("fibrillatory conduction"[26]). The identification of a spiral wave requires covering the coherent domain with a sufficient number of electrodes. This number depends on the location of the spiral wave with respect to the electrode array as well as the dynamics of the spiral tip. Consider again a rigidly rotating Archimedean spiral with a tip location that is within a square 2×2 electrode array with grid spacing Δx. This array can identify a spiral wave if the activation of the electrodes is sequential, either clockwise or counterclockwise. It is easy to see that if the tip is located exactly at the center of the array that the electrodes will display sequential activation with an interelectrode interval of $\tau/4$, independent of the grid spacing and spiral wavelength. Thus, in this case, it is possible to identify a spiral wave with only 4 electrodes, provided that the array covers the coherent domain. For non-central tip locations, the activation sequence depends on both the tip position as well as the grid spacing.

The requirement for grid spacing is most restrictive if the tip location is close to one of the electrodes. In that case, we can determine the activation time of this electrode and the activation time of its neighbor using Eq. (5). Choosing the tip location for the nearest electrode such that $x_1 = \delta$ and $y_1 = \varepsilon$ with $\delta \ll \varepsilon \ll 1$, we find that $t_1/\tau \approx 1/4 + k$. The activation time of the neighboring electrode that will be activated first can be found using $x_2 = -\Delta x$ and $y_2 = \varepsilon$, resulting in $t_2/\tau \approx 1/2 + k\text{-}\Delta x/\lambda_{spiral}$. For sequential activation, we demand $t_1 < t_2$, leading to the requirement $\Delta x < \lambda_{spiral}/4$. Note that this requirement can also be found using the geometric properties of an Archimedean spiral. Thus, as long as $\Delta x < \lambda_{spiral}/4 < L_{rotor}$, a 2×2 array should be able to identify a rigidly rotating spiral with negligible core size, provided that the spiral tip location falls within the array.

The above analysis is obviously not valid for spiral waves with a meandering tip or large core size. In this case, the relationship between L_{rotor} and the required minimum number of electrodes and maximum grid spacing is more difficult to determine and depends on the precise tip dynamics. Most likely, however, identification of these spiral waves require electrode arrays that are larger than 2 × 2. Identification of a meandering rotor also calls for a spatial extent of mapping that is larger than L_{tip}. After all, a rotor that moves in and out the field of view will result in activation patterns that are hard to interpret. If the precise location of the spiral tip path is not known *a priori*, as is the case in AF,[6,7] the entire cardiac chamber of interest should ideally be mapped.

Finally, the required temporal resolution depends on the spatial resolution of the employed grid, Δx, and needs to be such that activation between neighboring spatial elements can be distinguished. The results in the requirement that $\Delta t < \Delta x/v$, where v is the conduction velocity of the activation front.

2. Mapping focal sources

Focal sources originate at a discrete spatial origin and result in a centrifugal pattern of activation with a wavelength λ_{focal}, defined as the spatial separation between two successive centrifugal wavefronts (Fig. 1(c)). For a focal source propagating with a uniform velocity v, the activation times of electrode i at location x_i and y_i for a focal source with period T and located at x_0 and y_0 can be found as

$$t_i = \frac{\sqrt{(x_i - x_0)^2 + (y_i - y_0)^2}}{v} + nT (n = 0, 1, 2, ...) \quad (7)$$

In Fig. 1(d), we plot the circular isochrones corresponding to a focal source with $\lambda_{focal} = 4\Delta x$ as white lines, along with the corresponding isochronal regions. The wave speed and its period were chosen such that the focal wavelength is $\lambda_{focal} = 4\Delta x$, where Δx is the spatial discretization of the 8 × 8 grid, shown as black dots. We can again derive a stringent spatial resolution requirement by defining the maximum allowable Δx to be the spatial resolution for which isochronal regions are still spatially continuous. Following the same arguments as above, we find that this required resolution for N spatially continuous isochronal regions is $\Delta x = \lambda_{focal}/N$. The required temporal resolution for focal sources can again be estimated as $\Delta t \approx \Delta x/v$.

Finally, as for spiral waves, we can define a coherent domain, L_{focal}, which defines the tissue that is activated in a 1:1 fashion by the focal source. A 2 × 2 array will give identical electrode activation times, allowing for focal source identification, only if the source is located exactly in the middle of the array. For off-center locations, the activation times will be neither sequential nor identical, necessitating a larger array size to identify the focal source.

B. Experimental considerations

The spatial and temporal resolutions that result from the analysis above can be estimated based on animal studies and observations of human AF. In animal models of AF, the path of the spiral tip has a length scale (L_{tip}) ranging from 1 cm to 3 cm.[27–29] We therefore expect that for meandering spiral tips with the largest L_{tip}, the required resolution for accurately mapping the spiral tip will be much smaller that 1 cm while the required field of view needs to be larger that 3 cm × 3 cm. Also, in a canine model, a single rotor was found to control tissue with an area of >5 cm^2 (Ref. 30) and a spiral wavelength of >3 cm. Thus, mapping reentry with N = 4 isochronal regions for this spiral would require a spatial resolution of $\Delta x \approx 3/4 = 0.75$ cm.

In humans, both a lower bound of the wavelength of a spiral and a lower bound of the wavelength of a focal beat may be estimated from the product of minimum conduction velocity and shortest refractory period.[31] Note that this is an underestimate of the wavelength as defined earlier. In AF patients, minimum (dynamic) conduction velocity in left and right atria is $v_{min} \approx 40$ cm/s (Ref. 32) and minimum atrial refractory period ≈110 ms (Refs. 33 and 34) resulting in a minimum wavelength $\lambda_{min} = v_{min}T_{min} \approx 4.4$ cm. Thus, visualizing the spiral activation patterns using four isochronal regions will require a spatial resolution of $\Delta x \approx 1.1$ cm. Similarly, spatially resolved isochronal maps of focal beats with N = 4 regions will require a spatial resolution of $\Delta x \approx 1.1$ cm or smaller. Finally, the required temporal resolution can be estimated as the ratio of the spatial resolution and the maximum conduction velocity. Using a maximum conduction velocity of $v_{max} = 200$ cm/s (Ref. 35) and a spatial resolution of $\Delta x = 1.1$ cm, we find a required temporal resolution of $\Delta t = \Delta x/v_{max} \approx 5$ ms.

III. COMPUTER SIMULATIONS

To test these estimated resolution requirements, we constructed *in silico* data sets as described above. As a first test of our estimates, we generated a spiral wave reentry pattern in a 200 × 200 node simulation area with a physical size of 5 × 5 cm (Fig. 2(a)). The parameters of the model were chosen such that the coherent domain of the rotor spanned the entire simulation area (Fig. 2(a)) and that the period of the rotor was approximately 84 ms. Furthermore, the spiral is single-armed with a wavelength that was found to be $\lambda_{spiral} = 5.0$ cm. By computing the location of the spiral tip, using the algorithm of Ref. 23, we determined the spiral tip path. This path, shown in Fig. 2(a) in red, consists of a complex meandering trajectory with a length scale of $L_{tip} \approx 1$ cm. Note that the physical dimensions and timescale of the simulation can be altered by an appropriate rescaling of the parameters.

The activation times for each node were determined using a threshold (10% maximal V) and were stored with a temporal resolution of $\Delta t = 1$ ms. These activation times were then used to compute isochrones, defined as all points that were activated within a certain time interval ΔP. Four isochrones with interval $\Delta P = 1$ ms, separated by 20 ms, are shown in Fig. 2(a) in green. The resolution for this simulation is much smaller than the spiral wave length and the length scale of its tip. Thus, as expected, computing the

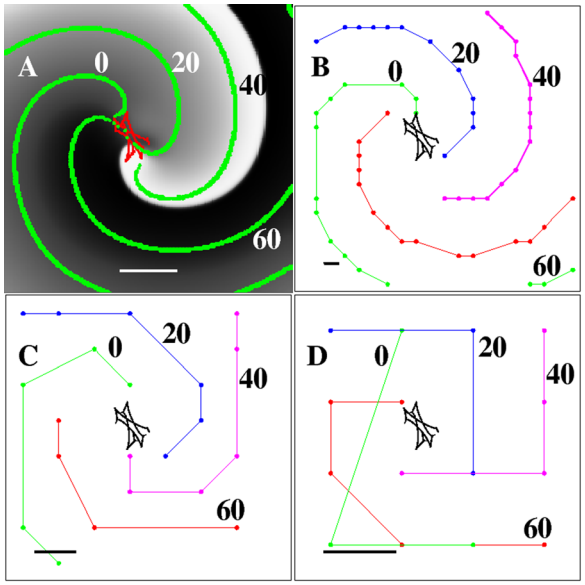

FIG. 2. Computer simulation of a single-armed rotor spanning the entire field of view. (A) Snapshot of the activation (t = 45 ms) of a clock-wise rotating rotor simulated on a 200 × 200 grid, corresponding to a 5 × 5 cm domain. The activation is plotted using a gray scale while the meandering spiral tip of the rotor is shown in red. The green symbols are isochrones, 20 ms apart, superimposed onto the snapshots. Scalebar = 1 cm. (B) Isochrones computed on a 20 × 20 grid that was obtained by spatially coarsening the original 200 × 200 grid. Isochrones are again 20 ms apart and the scalebar represents the spatial resolution (Δx = 2.5 mm). (C) Same as (B) but now using an 8 × 8 grid and a spatial resolution of Δx = 6.25 mm. (D) Same as (B) and (C), using a 4 × 4 grid and a spatial resolution of Δx = 12.5 mm. This illustrative reentry pattern was generated using the FK model of Ref. 42.

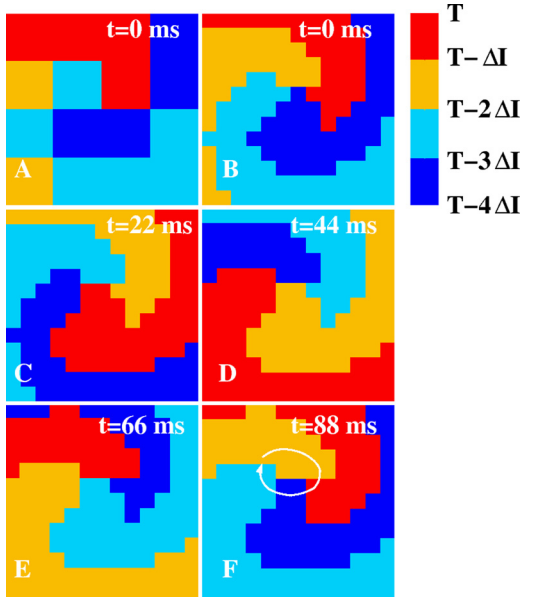

FIG. 3. Snapshots of isochronal maps computed using the data of Fig. 2(D). For visualization purposes, the 4 × 4 grid was bi-linearly interpolated. The activation of the grid points are binned in ΔI = 22 ms isochrone intervals (corresponding to approximately a quarter of the spiral period) and are color coded according to the colorbar. For example, red corresponds to all grid points that are activated in the first isochrone interval immediately preceding the snapshot at time T (i.e., in the interval (T- ΔI,T)). The white line in (F) indicates the direction of rotation of the rotor.

activation times at this resolution is sufficient to easily identify the rotor, its domain, and its spiral tip path.

Next, we progressively increased the distance between the locations where we sampled the activation times. This downsampling of the data results in an increase in the spatial resolution without having to re-run the computational model with a larger Δx. Using the activation times on this coarsened grid, we again computed isochrones separated by 20 ms, using progressively larger intervals ΔP. In Figs. 2(b)–2(d), we show the results for spatial resolutions of Δx = 2.5 mm (20 × 20 grid), Δx = 6.25 mm (8 × 8 grid), and Δx = 12.5 mm (4 × 4 grid). A visual inspection of the isochrones reveals that for these discretizations, the spiral tip path is no longer resolved. This is expected since this complex trajectory requires a resolution that is much smaller than L_{tip}.

However, isochrones for all values of Δx demonstrate rotational activity of the rotor. This can be seen more clearly by creating a sequence of isochronal maps. For visualization purposes, these maps are created by bi-linearly interpolating the activation times between the electrodes, adding 3 points between two neighboring grid points in each direction. Five snapshots of these maps, separated by 22 ms, are shown in Figs. 3(b)–3(f) for the coarsest grid in Fig. 2 (Δx = 12.5 mm). As a comparison, the non-interpolated isochronal map corresponding to Fig. 3(b) is shown in Fig. 3(a). These snapshots show that the rotational activation around the rotor core location can be identified, even with a spatial resolution of Δx = 12.5 mm. This result is agreement with the theoretical consideration above: since the rotor wavelength is 5.0 cm, we expect that for four isochronal regions, the minimum resolution is 5/4 = 1.25 cm and that a resolution of 1.25 cm will be sufficient to resolve the reentry pattern.

A second simulation shows a stable rotor with wavelength $\lambda = 3.2$ cm, spiral tip path of $L_{tip} \approx 1$ cm, and a period of approximately $\tau = 90$ ms depicted at Δx = 0.5 mm (Fig. 4(a)). The coherent domain of the rotor is $L_{rotor} = 6$ cm, beyond which the rotor destabilizes and breaks down. As in previous simulation studies, this break-down ("fibrillatory conduction") is achieved by changing the model parameters in part of the tissue.[36,37] Specifically, we chose a different value of one of the parameters (τ_r) in the outer region of the computational domain (defined as the region that has a distance of 5 cm or more from the center of the domain). Note that a similar break-down can also be achieved in homogenous tissue.[24]

Based on our estimates, we expect that a spatial resolution that is much smaller than L_{tip} will be necessary to accurately track the spiral tip path. However, to simply identify the rotor, we expect to be able to coarsen the simulation results to a spatial resolution of $\Delta x \approx \lambda/5 = 6.4$ mm if we use five isochronal regions. In Figs. 4(b) and 4(c), we show snapshots of an isochronal map using N = 5 isochronal regions with interval ΔI = 20 ms of the simulation of Fig. 4(a), for Δx = 6 mm (b), and Δx = 12.5 mm (c), corresponding to a 25 × 25 grid and 12 × 12 grid, respectively. As in Fig. 3, the activation times were bi-linearly interpolated. The isochronal map at the higher spatial resolution clearly shows the existence of a rotor, in agreement with theoretical estimates. The

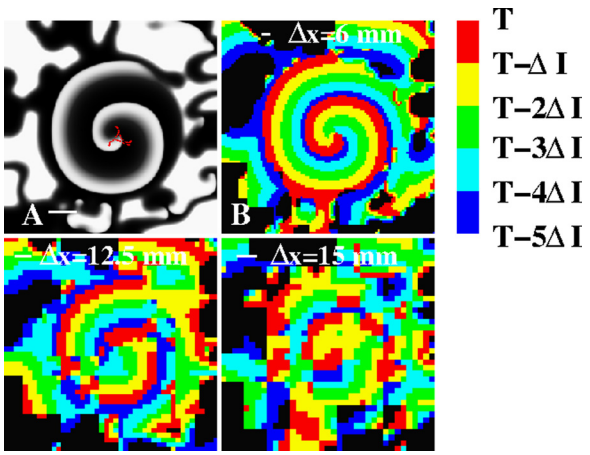

FIG. 4. A simulated stable counterclockwise rotating rotor and its break-down. (A) A 15 × 15 cm computational domain, with spatial resolution $\Delta x = 0.5$ mm, contains a stable rotor with a meandering spiral tip path shown in red. The rotor was simulated using the 3-variable FK model (parameter set #3 from Ref. 24) and the break-down of the spiral was generated by assigning a different value of one of the parameters in the outer region of the computational domain ($\tau_r = 0.4$ vs. $\tau_r = 0.27$). Scalebar = 2 cm. (B) Isochronal map using a spatial resolution of $\Delta x = 6$ mm, as indicated by the scalebar, using the data from A. (C) Snapshot of an isochronal map on a 12 × 12 grid. The scale bar represents the spatial resolution ($\Delta x = 12.5$ mm). (D) Snapshot of an isochronal map on a 15 × 15 grid from an animated sequence. All isochronal maps used an isochronal interval of $\Delta I = 20$ ms (enhanced online) [URL: http://dx.doi.org/10.1063/1.4807098.1].

further coarsening of resolution, however, reduces the ability to identify a rotational pattern in a single snapshot (Fig. 4(c)) although a series of successive snapshots may still enable detection of the rotor. This is demonstrated in Fig. 4(d), which shows a snapshot of an animation of successive isochronal maps at resolution $\Delta x = 15$ mm.

A third simulation addresses the required resolution for resolving a focal source. For this simulation, a fixed node at the center of a 300 × 300 computational grid with $\Delta x = 0.5$ mm was stimulated with a period of 100 ms (Fig. 5(a)). As in the simulation of Fig. 4, we introduced fibrillatory conduction by choosing heterogeneous model parameters, leading to a coherent domain of $L_{beat} = 7$ cm and a wavelength of $\lambda_{focal} \approx 3$ cm. Thus, the required spatial resolution is set by this wavelength for N = 4 isochronal regions should be $\Delta x \approx \lambda_{focal}/4 = 0.75$ cm or smaller. Indeed, an isochronal map at a resolution of $\Delta x = 7.5$ mm (20 × 20 grid, $\Delta I = 25$ ms) clearly shows a centrifugal activation pattern, consistent with our estimate (Fig. 5(b)). Further spatially coarsening the data, however, leads to activation patterns that are not readily identifiable as target patterns. This is shown in Fig. 5(c), where we plot the N = 4 isochronal map for a resolution of $\Delta x = 15$ mm (10 × 10 grid).

IV. VALIDATION OF RESOLUTION ESTIMATES IN CLINICAL ATRIAL FIBRILLATION

We have recently studied activation patterns of patients with persistent and paroxysmal AF referred for ablation.[12] Detailed information regarding the characteristics of the patient population can be found in Ref. 20 while our mapping technique is further described in Ref. 21.

Briefly, mapping is accomplished using two 64-pole contact electrode catheters in the form of "baskets" that are advanced to the right atrium (RA) and, after trans-septal puncture, to the left atrium (LA). The baskets, along with the relevant anatomy, are schematically shown in Fig. 6(a). Along each spline of the basket, the interelectrode distance is 4–5 mm, while the distance between the splines can be estimated as <1 cm at the equator of the basket and <4 mm near its poles. Thus, this technique produces activation maps on an 8 × 8 grid with a spatial resolution between 0.4 and 1 cm.

Multisite electrograms are recorded with a temporal resolution of 1 ms (filtered at 0.05–500 Hz at the source recording). From the resolution estimates above, we anticipated that this temporal and spatial resolution should distinguish activation events between neighboring electrodes. AF data are exported digitally over a period of >30 min. Multipolar AF signals are then analyzed by filtering electrograms to exclude noise and far-field signals, followed by determination of the activation times at each electrode over successive cycles to map electrical propagation in AF.[21]

Data from multiple institutions have used this system to show that human AF is perpetuated by a small number of rotors or focal sources.[20,38] Unexpectedly, these sources were found to be stable over a prolonged period of time (hours to months). Empirically, the mechanistic relevance of these sources to sustaining AF was recently demonstrated by brief targeted ablation only at sources (Focal Impulse and Rotor Modulation, FIRM), which acutely terminated AF with subsequent inability to induce AF ("non-reinducibility")

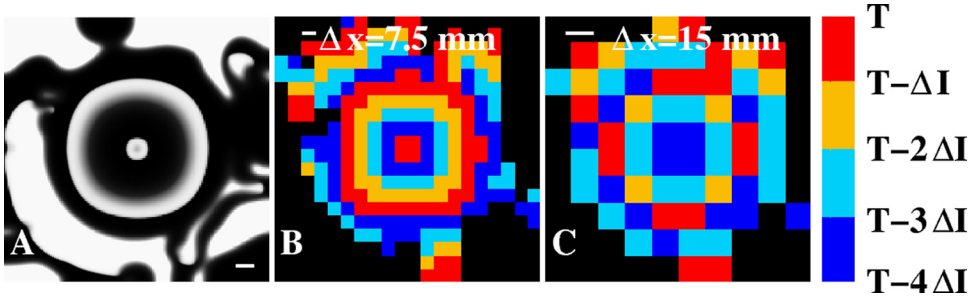

FIG. 5. Focal pattern in a simulation. (A) A snapshot of the tissue activation of a focal source located at the center of the 15 × 15 cm domain (model parameters are as in Fig. 4). Scalebar = 1 cm. (B) Isochronal map using four $\Delta I = 25$ ms isochronal intervals and a spatial resolution of $\Delta x = 7.5$ mm (indicated by the scale bar). Four separate and spatially continuous isochronal regions can be clearly identified. (C) Isochronal map using four $\Delta I = 25$ ms isochronal intervals and a spatial resolution of $\Delta x = 15$ mm (indicated by the scale bar). The centrifugal activation pattern can no longer be identified at this resolution. Black corresponds to grid points that were not activated in any of the four preceding isochronal intervals.

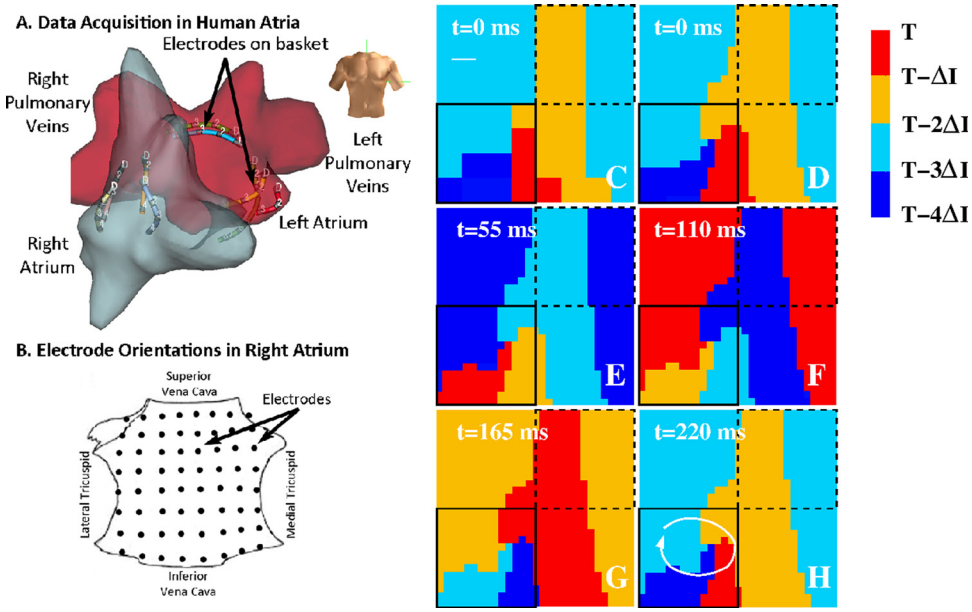

FIG. 6. (A) Schematic depiction of the data acquisition in patients. The atria are presented in an anterior (frontal) view (see torso) with the left atrium shown in red and the right atrium in gray. Some of the contact electrodes, inserted into the atria to record tissue activation, are shown. (B) The orientation of the electrodes are shown in the RA, which is opened between its poles with tricuspid annulus opened laterally and medially (the LA is opened along its equator, with mitral annulus opened superiorly and inferiorly[21]). ((C)-(H)) Isochronal maps of the RA of a patient with persistent AF. The non-interpolated data on a 8×8 electrode grid with spatial resolution between 0.4 and 1 cm are shown in (C) while in (D)–(H), and in Figs. 7 and 8, the electrode grid was bi-linearly interpolated for visualization purposes. The maps reveal a rotor with period $\tau = 220$ ms in the low RA, as indicated by the white line if (F) resulting in $\Delta I = \tau/4 = 55$ ms. The solid square represents the minimal field of view and location that is required to capture the rotor. The dashed square shows an identically sized field of view at a different location that is not able to determine the existence of a rotor. The white bar in (C) represents the interelectrode spacing.

in a majority of patients.[20] Importantly, the long-term results of this novel ablation approach have recently been shown to be substantially better than conventional ablation of empirical anatomic targets without knowledge of the propagation patterns in any given individual.[20]

We will now examine the clinical data using isochronal maps as described above. As in our previous work, activation is visualized in panels where the RA is opened vertically through the tricuspid valve such that the left edge of each panel indicates the lateral tricuspid annulus and the right edge indicates the septal tricuspid annulus.[12,20,39] A schematic illustration of the anatomical position of the electrode grid in the patients is shown in Fig. 6(b). In Figs. 6(c)–6(h), we plot a sequence of isochronal maps at $\Delta I = 55$ ms isochrone intervals in the right atrium of a patient with persistent AF. The activation map is visualized on an 8×8 grid in (c) and has been bi-linearly interpolated in ((d)-(h)). The maps reveal a spatially localized rotor in the low RA (white line in (h)) with a coherent domain that is larger than the visualization domain. Thus, similar to rotor shown in Figs. 2 and 3, this is a single-armed rotor with a coherent domain that spans the entire field of view with a wavelength that is larger or comparable to the size of this domain. Although the precise spiral tip path is difficult to determine from Fig. 6, its estimated length scale is much smaller than the coherent domain and the wavelength. Interestingly, the location of the rotor was conserved over many rotations, suggesting a role of spatial heterogeneities in maintaining the spatio-temporal organization of AF.

We can now determine if the mapping results for this pattern are consistent with our derived estimates. For an isochronal map with $N = 4$ regions, the required spatial resolution can be estimated as $\Delta x \approx \lambda_{\text{spiral}}/4$. For a wavelength equal to the size of the field of view, this requires having at least 4 electrodes in either direction. Therefore, an 8×8 grid will capture the rotor if placed over the spiral tip path, consistent with our results. Fig. 6 also demonstrates the importance of the location of the field of view. The solid square in Figs. 6(c)–6(h) represents a 4×4 grid and shows that the data within this grid are sufficient to identify the rotor. The dashed square in Figs. 6(c)–6(h) represents a 4×4 mapping array that is identical in size but centered in an "incorrect position" away from the spiral tip path. Clearly, limiting the field of view to this area will not accurately capture the rotor, even if the spatial resolution were increased.

In Fig. 7, we show a sequence of isochronal maps in the left atrium, at $\Delta I = 50$ ms isochrone intervals and $N = 5$ regions, during paroxysmal AF in a separate patient. For this patient, 64 basket poles resulted in an 8×8 grid displayed by opening the left atrium horizontally through the mitral valve, with the top edge of each panel indicating the superior mitral annulus and the bottom edge indicating the inferior mitral annulus.[21] Panels (A)-(F) show isochronal snapshots every 50 ms, and reveal a rotor that controls only the lower part of the left atrium (white line in (F)), with the remaining atrium showing complex spatio-temporal patterns ("fibrillatory conduction"). Again, the wavelength of the rotor is larger than the size of the field of view. Thus, the number of electrodes and its corresponding spatial resolution are sufficient to capture the rotor. As for the rotor of Fig. 6, the pattern was conserved for a significant period of time (at least 2 h (Ref. 12)), possibly due to spatial heterogeneities.

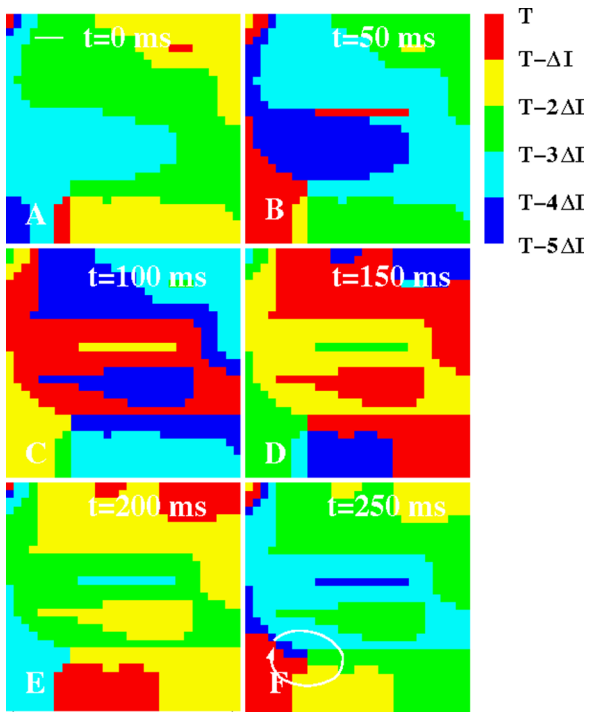

FIG. 7. Isochronal maps of the LA of a patient with paroxysmal AF ($\Delta I = 50$ ms). A rotor is visible in the low LA, visualized by the white line in (F), with more complex dynamics in the upper portion of the LA. The white bar in (A) represents the interelectrode spacing.

A third clinical example is shown in Fig. 8 where we plot three snapshots of isochronal activation in the LA of a patient with paroxysmal AF. These snapshots were chosen such that the maps show activation in at least five preceding 10 ms isochrone intervals and capture three successive activations. The maps clearly show centrifugal activation radiating from a localized source with a period of approximately 190 ms, thus capturing a focal source pattern that was located at roughly the center of the field of view. Again working backwards, we can estimate the required resolution for this activation pattern. The focal source has a coherent domain that spans the entire field of view. Furthermore, the wavelength of the focal beat can be estimated to be at least the size of the field of view since an activation front reaches the boundary within half a period. Thus, the required resolution for five isochronal regions translates into five electrodes spanning the field of view. Clearly, the clinical 8×8 basket fulfills this requirement and has sufficient spatial resolution to accurately capture focal source activation.

V. DISCUSSION

Accurate mapping of spatio-temporal patterns during human arrhythmias is challenging and requires recording methods carefully tailored to the pathophysiology of the arrhythmia being studied. In this study, we provide theoretical, *in silico,* and clinical data to show that spiral wave reentry (rotors) and repetitive focal sources recently shown to sustain human atrial fibrillation can be resolved with a spatial resolution of millimeters to $\approx$1 cm.

Since optical dye fluorescence techniques employed in animal studies cannot be used in humans due to concerns over toxicity, contact electrode arrays are the most common mapping modality[13,14] although non-invasive and non-contact techniques using the inverse solution have been developed.[40,41] Contact arrays have been used to determine the spatio-temporal organization during human AF.[20,21] These studies provide a lower spatial resolution than optical studies in animals, yet have identified spatial non-uniformities in human AF consistent with localized sources.[13,14]

Our derived theoretical estimates are based on observations in the literature that the rotor wavelength is larger than the length scale of the spiral tip path, and that the coherent domain of the rotor or focal source spans a significant portion of the field of view. Our derived theoretical estimate for the spatial resolution is based on rigidly rotating Archimedean spirals. The required spatial resolution for non-rigidly rotating spirals is likely to be more stringent although our simulations show that the theoretical requirement still works reasonably well for meandering spirals. Furthermore, noise in the electrode recordings and their position will also affect the required resolution. Our analysis of the clinical data, however, verify that the spatial and temporal resolution of our recently reported mapping approach,[21] which uses bi-atrial basket catheters to provide 4–10 mm spatial and 1 ms temporal resolution, are sufficient to capture AF rotors and focal sources, particularly if depicted as a series of propagation maps (movies). Data from multiple institutions have used this system to show that human AF is perpetuated by a small number of rotors or focal sources.[20,38] Unexpectedly, these sources were found to be stable over a prolonged period of time (hours to months). Empirically, the mechanistic relevance of these sources to sustaining AF was recently demonstrated by brief targeted ablation only at sources (Focal Impulse and Rotor Modulation, FIRM), which acutely terminated AF with subsequent inability to induce AF ("non-reinducibility") in a majority of patients (86%).[20] Importantly, the long-term results of

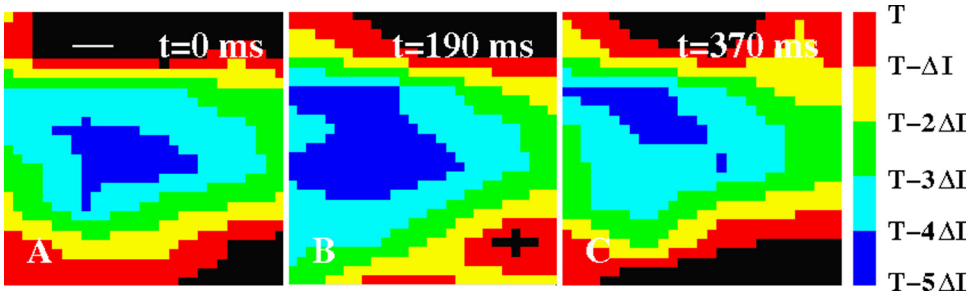

FIG. 8. Isochronal maps of the LA of a patient with paroxysmal AF ($\Delta I = 50$ ms). The maps show three successive focal sources from an origin, in the posterior LA mid-way between the pulmonary vein pairs and >2 cm from each pulmonary vein ostium, at the indicated times. Black corresponds to grid points that were not activated in any of the five preceding isochronal intervals. The white bar in (A) represents the interelectrode spacing.

this novel ablation approach have recently been shown to be substantially better than conventional ablation of empirical anatomic targets without knowledge of the propagation patterns in any given individual (82.4% vs. 44.9%).[20]

Clearly, no mapping technique can resolve spatial events with a length scale smaller than the inter-electrode spacing. For example, it is impossible to distinguish a spiral wave with a wavelength smaller than the inter-electrode spacing nor is it possible to precisely map the spiral tip path if its lengthscale is smaller than the spatial resolution of mapping.[29] Although this imposes a potential mapping limit, re-entry on this small scale may be uncommon in human atria since wavelength considerations suggest a minimum wavelength of ≈4–5 cm.[31–34] Moreover, the inability to precisely resolve the spiral tip path may be of less clinical relevance if the approximate center of rotation can be identified, since a single ablation lesion typically covers a region of diameter 5–7 mm.[20] Finally, we note that although we have focused on atrial wave propagation, our theoretical and computational estimates should also be valid for spiral waves in the ventricles, provided that we use parameters applicable to ventricular tissue and that our analyses would be restricted to the mapping plane(s).

We anticipate that these mapping considerations will become central to designing further mechanistic and therapeutic studies of human AF and other complex clinical arrhythmias.

ACKNOWLEDGMENTS

This work was supported by NIH Grants NHLBI HL70529 (S.M.N.), HL083359 (S.M.N. and W.J.R.), and HL103800 (S.M.N.).

[1]V. Fuster *et al.*, "ACC/AHA/ESC 2006 Guidelines for the Management of Patients with Atrial Fibrillation: A report of the American College of Cardiology/American Heart Association Task Force on Practice Guidelines and the European Society of Cardiology Committee for Practice Guidelines (Writing Committee to Revise the 2001 Guidelines for the Management of Patients With Atrial Fibrillation): Developed in collaboration with the European Heart Rhythm Association and the Heart Rhythm Society," Circulation **114**, e257–e354 (2006).
[2]S. Lazar, S. Dixit, F. E. Marchlinski, D. J. Callans, and E. P. Gerstenfeld, "Presence of left-to-right atrial frequency gradient in paroxysmal but not persistent atrial fibrillation in humans," Circulation **110**, 3181–3186 (2004).
[3]E. P. Gerstenfeld, A. V. Sahakian, and S. Swiryn, "Evidence for transient linking of atrial excitation during atrial fibrillation in humans," Circulation **86**, 375–382 (1992).
[4]K. Nanthakumar *et al.*, "Optical mapping of Langendorff-perfused human hearts: Establishing a model for the study of ventricular fibrillation in humans," Am. J. Physiol. Heart circ. Physiol. **293**, H875–880 (2007).
[5]V. V. Fedorov *et al.*, "Effects of KATP channel openers diazoxide and pinacidil in coronary-perfused atria and ventricles from failing and non-failing human hearts," J. Mol. Cell. Cardiol. **51**, 215–225 (2011).
[6]S. Nattel, "New ideas about atrial fibrillation 50 years on," Nature **415**, 219–226 (2002).
[7]M. Vaquero, D. Calvo, and J. Jalife, "Cardiac fibrillation: From ion channels to rotors in the human heart," Heart Rhythm **5**, 872–879 (2008).
[8]K. Ryu *et al.*, "Mapping of atrial activation during sustained atrial fibrillation in dogs with rapid ventricular pacing induced heart failure: Evidence for a role of driver regions," J. Cardiovasc. Electrophysiol. **16**, 1348–1358 (2005).
[9]J. Kalifa *et al.*, "Mechanisms of wave fractionation at boundaries of high-frequency excitation in the posterior left atrium of the isolated sheep heart during atrial fibrillation," Circulation **113**, 626–633 (2006).
[10]A. C. Skanes, R. Mandapati, O. Berenfeld, J. M. Davidenko, and J. Jalife, "Spatiotemporal periodicity during atrial fibrillation in the isolated sheep heart," Circulation **98**, 1236–1248 (1998).
[11]N. M. de Groot *et al.*, "Electropathological substrate of longstanding persistent atrial fibrillation in patients with structural heart disease: Epicardial breakthrough," Circulation **122**, 1674–1682 (2010).
[12]S. M. Narayan, D. E. Krummen, M. W. Enyeart, and W. J. Rappel, "Computational mapping identifies localized mechanisms for ablation of atrial fibrillation," PloS one **7**, e46034 (2012).
[13]T.-J. Wu *et al.*, "Simultaneous biatrial computerized mapping during permanent atrial fibrillation in patients with organic heart disease," J. Cardiovasc. Electrophysiol. **13**, 571–577 (2002).
[14]J. Sahadevan *et al.*, "Epicardial mapping of chronic atrial fibrillation in patients: Preliminary observations," Circulation **110**, 3293–3299 (2004).
[15]M. A. Allessie *et al.*, "Electropathological substrate of long-standing persistent atrial fibrillation in patients with structural heart disease: Longitudinal dissociation," Circ. Arrhythmia Electrophysiol. **3**, 606–615 (2010).
[16]R. A. Winkle, R. H. Mead, G. Engel, M. H. Kong, and R. A. Patrawala, "Trends in atrial fibrillation ablation: Have we maximized the current paradigms?," J. Interv. Card. Electrophysiol. **34**, 115–123 (2012).
[17]A. L. Waldo and G. K. Feld, "Inter-relationships of atrial fibrillation and atrial flutter mechanisms and clinical implications," J. Am. College Cardiol. **51**, 779–786 (2008).
[18]K. Hall and L. Glass, "Locating ectopic foci," J. Cardiovasc. Electrophysiol. **10**, 387–398 (1999).
[19]K. Hall and L. Glass, "How to tell a target from a spiral: The two probe problem," Phys. Rev. Lett. **82**, 5164–5167 (1999).
[20]S. M. Narayan *et al.*, "Treatment of atrial fibrillation by the ablation of localized sources: CONFIRM (Conventional Ablation for Atrial Fibrillation With or Without Focal Impulse and Rotor Modulation) trial," J. Am. College Cardiol. **60**, 628–636 (2012).
[21]S. M. Narayan, D. E. Krummen, and W. J. Rappel, "Clinical mapping approach to diagnose electrical rotors and focal impulse sources for human atrial fibrillation," J. Cardiovasc. Electrophysiol. **23**, 447–454 (2012).
[22]N. Wiener and A. Rosenblueth, "The mathematical formulation of the problem of conduction of impulses in a network of connected excitable elements, specifically in cardiac muscle," Arch. Inst. Cardiol. Mex **16**, 205–265 (1946).
[23]F. Fenton and A. Karma, "Vortex dynamics in three-dimensional continuous myocardium with fiber rotation: Filament instability and fibrillation," Chaos **8**, 20–47 (1998).
[24]F. H. Fenton, E. M. Cherry, H. M. Hastings, and S. J. Evans, "Multiple mechanisms of spiral wave breakup in a model of cardiac electrical activity," Chaos **12**, 852–892 (2002).
[25]S. Zlochiver, M. Yamazaki, J. Kalifa, and O. Berenfeld, "Rotor meandering contributes to irregularity in electrograms during atrial fibrillation," Heart Rhythm **5**, 846–854 (2008).
[26]J. Jalife, O. Berenfeld, and M. Mansour, "Mother rotors and fibrillatory conduction: A mechanism of atrial fibrillation," Cardiovasc. Res. **54**, 204–216 (2002).
[27]B. C. Hill and K. R. Courtney, "Design of a multi-point laser scanned optical monitor of cardiac action potential propagation: Application to microreentry in guinea pig atrium," Ann. Biomed. Eng. **15**, 567–577 (1987).
[28]C. Kirchhof *et al.*, "Regional entrainment of atrial fibrillation studied by high-resolution mapping in open-chest dogs," Circulation **88**, 736–749 (1993).
[29]R. E. Ideker *et al.*, "Can mapping differentiate microreentry from a focus in the ventricle?," Heart Rhythm **6**, 1666–1669 (2009).
[30]E. M. Cherry and F. H. Fenton, "Visualization of spiral and scroll waves in simulated and experimental cardiac tissue," New J. Phys. **10**, 125016 (2008).
[31]P. Rensma, M. Allessie, W. Lammers, F. Bonke, and M. Schalij, "Length of excitation wave and susceptibility to reentrant atrial arrhythmias in normal conscious dogs," Circ. Res. **62**, 395–410 (1988).
[32]G. G. Lalani *et al.*, "Atrial conduction slows immediately before the onset of human atrial fibrillation: A bi-atrial contact mapping study of transitions to atrial fibrillation," J. Am. College Cardiol. **59**, 595–606 (2012).
[33]S. M. Narayan, M. R. Franz, P. Clopton, E. J. Pruvot, and D. E. Krummen, "Repolarization alternans reveals vulnerability to human atrial fibrillation," Circulation **123**, 2922–2930 (2011).
[34]S. M. Narayan, D. Kazi, D. E. Krummen, and W. J. Rappel, "Repolarization and activation restitution near human pulmonary veins and atrial fibrillation

initiation: A mechanism for the initiation of atrial fibrillation by premature beats," J. Am. College Cardiol. **52**, 1222–1230 (2008).
[35]D. Harrild and C. Henriquez, "A computer model of normal conduction in the human atria," Circ. Res. **87**, E25–E36 (2000).
[36]A. Baher *et al*., "Short-term cardiac memory and mother rotor fibrillation," Am. J. Physiol. **292**, H180–H189 (2007).
[37]F. H. Samie *et al*., "Rectification of the background potassium current: A determinant of rotor dynamics in ventricular fibrillation," Circ. Res. **89**, 1216–1223 (2001).
[38]K. Shivkumar, K. A. Ellenbogen, J. D. Hummel, J. M. Miller, and J. S. Steinberg, "Acute termination of human atrial fibrillation by identification and catheter ablation of localized rotors and sources: First multicenter experience of focal impulse and rotor modulation (FIRM) ablation," J. Cardiovasc. Electrophysiol. **23**, 1277–1285 (2012).
[39]S. M. Narayan, J. Patel, S. K. Mulpuru, and D. E. Krummen, "Focal impulse and rotor modulation (FIRM) of sustaining rotors abruptly terminates persistent atrial fibrillation to sinus rhythm with elimination on follow-up," Heart Rhythm **9**(9), 1436–1439 (2012).
[40]P. S. Cuculich *et al*., "Noninvasive characterization of epicardial activation in humans with diverse atrial fibrillation patterns," Circulation **122**, 1364–1372 (2010).
[41]J. Zhao *et al*., "Electropathological substrate detection of persistent atrial fibrillation—a novel method to analyze unipolar electrograms of noncontact mapping," Conf. Proc. IEEE Eng. Med. Biol. Soc. 2011, 1471–1474.
[42]F. H. Fenton, E. M. Cherry, A. Karma, and W. J. Rappel, "Modeling wave propagation in realistic heart geometries using the phase-field method," Chaos **15**, 13502 (2005).